

Proteinaceous Nanoshells with Quasicrystalline Local Order

Sergei B. Rochal¹, Aleksey S. Roshal¹, Olga V. Konevtsova¹, and Rudolf Podgornik^{2,3,4}

¹*Faculty of Physics, Southern Federal University, 344090 Rostov-on-Don, Russia*

²*School of Physical Sciences and Kavli Institute for Theoretical Sciences, University of Chinese Academy of Sciences, 100049 Beijing, China*

³*CAS Key Laboratory of Soft Matter Physics, Institute of Physics, Chinese Academy of Sciences, 100190 Beijing, China*

⁴*Wenzhou Institute of the University of Chinese Academy of Sciences, Wenzhou, 325000 Zhejiang, China*

 (Received 27 March 2024; revised 28 May 2024; accepted 28 June 2024; published 5 August 2024)

Among various proteinaceous nanocontainers and nanoparticles, the most promising ones for various applications in nano- and medical science appear to be those whose structures differ fundamentally from icosahedral viral capsids described by the paradigmatic Caspar-Klug model. By analyzing such anomalous assemblies represented in the Protein Data Bank, we identify a series of shells with square-triangular local order and find that most of them originate from short-period approximants of a dodecagonal tiling consisting of square and triangular tiles. Examining the nonequilibrium assembly of such packings, we propose a new method for obtaining periodic square-triangle approximants and then construct the simplest models of tetragonal, octahedral, and icosahedral shells based on cubic and icosahedral nets cut from the approximant structures. Since gluing the nets can change the distances between adjacent vertices of the resulting shell, we introduce an effective energy, the minimization of which equalizes these distances. While the obtained spherical polyhedra reproduce the structures of experimentally observed protein shells and nanoparticles, the principles of protein organization that we lay out, and the ensuing structural models, can help to discover and investigate similar systems in the future.

DOI: [10.1103/PhysRevX.14.031019](https://doi.org/10.1103/PhysRevX.14.031019)

Subject Areas: Soft Matter

I. INTRODUCTION

The first quasicrystal (QC) discovered in the Al-Mn alloy about 40 years ago [1] had icosahedral symmetry, which is excluded for crystals on general grounds. Over the next decade, it was found that various icosahedral, octa-, deca-, and dodecagonal QCs are quite common for binary and ternary metal compounds [2]. Subsequently, QCs were revealed also in a number of soft-matter systems, among which one can highlight dendritic liquid quasicrystals formed from complex treelike molecules [3], colloidal nanocrystals self-assembling in an aqueous solution from micelles with core-shell structure [4], various polymer QCs [5,6], and other similar systems [7–9].

Unlike crystals, the structure of which is obtained by periodically repeating a unit cell, QCs are incommensurate structures, in which one can distinguish two (or several) “unit cells” referred to as tiles and arranged in an aperiodic manner. Structures of icosahedral protein viral shells

(capsids) can also be represented as spherical packings of certain tiles. In the most typical case, as discussed by Caspar and Klug (CK), a capsid is modeled as a packing of pentamers and hexamers [10]. These tiles (usually referred to as capsomers) consist of five and six individual proteins, respectively, and their centers form a trigonal order on a spherical surface [11,12].

Some structures of small anomalous viral capsids violate the CK model and can be represented in another QC-like manner, consisting of rhombuses, kites [13], or some other tiles [14–16]. However, the “generic” relation between a planar quasicrystalline order and the arrangement of proteins in a spherical shell was uncovered only in the case of bovine papillomavirus (*Papillomaviridae* family) capsid structure [17]. This capsid is represented as a dodecahedron, and the positions of individual proteins within its facets were obtained by a nonlinear phason strain of a planar decagonal tiling [15].

Anomalous protein shells of nonviral origin are also known. In some cases, these shells are described in terms of triangular and square tiles and concurrently resemble both Archimedean solids and planar tilings typical of many soft-matter systems [18]. Such spherical structures self-assembling from 24 proteins are shown in Figs. 1(a) and 1(c), while location of individual proteins in these shells is

Published by the American Physical Society under the terms of the Creative Commons Attribution 4.0 International license. Further distribution of this work must maintain attribution to the author(s) and the published article's title, journal citation, and DOI.

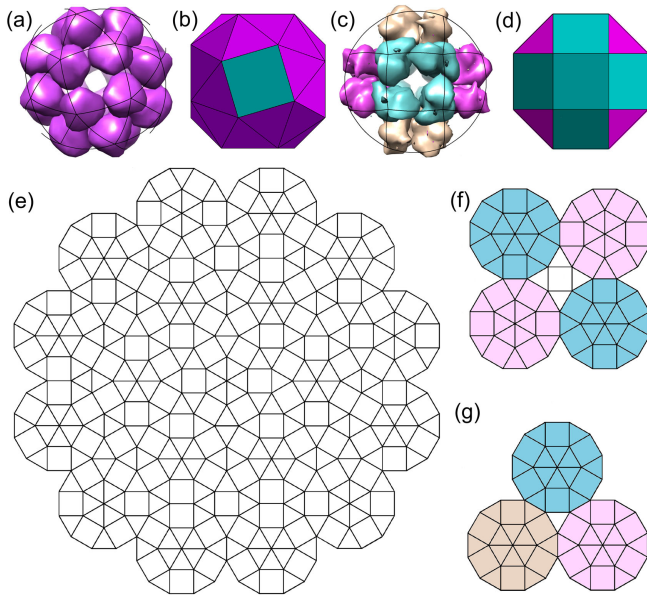


FIG. 1. S-T order on a spherical shell and on a plane. (a) Vitamin E transfer nanoparticle composed of 24 individual proteins (6ZPD). (b) Snub cube with 24 vertices, which are arranged in six square and 32 triangular tiles. (c) Chimallin (7SQQ). (d) Rhombicuboctahedron with 24 vertices, which form 18 square and eight triangular tiles. (e) Fragment of dodecagonal S-T tiling. (f), (g) Conjugation of four and three simple dodecagonal clusters called wheels.

characterized by a snub cube and rhombicuboctahedron geometry, respectively; see Figs. 1(b) and 1(d). Along with these assemblies, in the Protein Data Bank (PDB) [19] one can find many structurally similar shells and nanoparticles. Typical examples of the shells with triangular and square tiles are a hollow sphere from 24 identical sulfur oxygenase reductase monomers, the structure of imidazoleglycerolphosphate dehydratase, and the octahedral apoferritin nanocage. These and structurally analogous protein complexes can interact with DNA [20,21], act as enzymes [22,23], or serve as nanocontainers for various molecules including iron [24,25], iron-sulfur [26], vitamin E [27], and even misfolded proteins [28]. While there exist other shells, e.g., the recently discovered polymorphic encapsulation system based on *Aquifex aeolicus* lumazine synthase (AaLs) [29,30] that are structurally different, it is nevertheless easy to verify that the mass centers of pentamers comprising these shells are located approximately at the vertices of square and triangular tiles, which in turn are organized into spherical shells with tetrahedral and icosahedral symmetries.

We believe that the wide range of functionalities of the abovementioned proteinaceous nanoassemblies is due to their unusual structure, and therefore, in the main part of this article we examine even more proteinaceous shells with analogous square-triangular (S-T) local order. The main aim of our study is to reveal the generic relation between the considered spherical structures and planar

quasicrystalline tilings of appropriate types. As we show, most of these shells originate from linear periodic approximants of the dodecagonal S-T tiling; see Fig. 1(e). Since the number of the short-period S-T approximants turns out to be very limited, we build all the simplest models of tetragonal, octahedral, and icosahedral shells based on the dodecagonal S-T order. Some of these shells have already been experimentally observed, while the rest of our predictions are likely to be discovered in the coming years.

Because of the lack of theoretical methods to generate planar S-T packing, in the first part of the article, we propose a new way to construct such tilings including periodic approximants. Our method is based on the model of nonequilibrium cluster growth [31]. Within our approach, a new particle can attach to the growing cluster only in those positions, which are separated from the nearest occupied ones by at least one of 12 orientationally equivalent translations. The choice of the attachment position is based on the Boltzmann distribution function that depends on the ratio between binding energies calculated for different attachment options and thermal energy. Introduction of the effective binding energy based on the concepts of n -dimensional (nD) crystallography allows us to efficiently construct S-T periodic approximants, including those that cannot be obtained by the inflation method [32,33]. In the second part of the article, we then discuss how the obtained periodic approximants are transferred onto the sphere and compare the constructed shells with the experimentally observed ones. Here, we also propose structural models of yet undiscovered nanoshells with local S-T dodecagonal order and consider the proteinaceous nanoparticles originating from the octagonal tiling.

II. SELF-ASSEMBLY OF PLANAR SQUARE-TRIANGLE STRUCTURES

Constructing approximants of the planar S-T dodecagonal tiling [Fig. 1(e)] is not a trivial task. The original tiling is obtained exclusively by the inflation transformation [32], while the methods allowing regular construction of periodic approximants are based on a linear phason strain and developed only for those quasicrystalline tilings, which can be obtained by a projection from the nD space. However, known projection algorithms lead to the dodecagonal tilings that contain along with squares and triangles other tiles, for example, shields or narrow rhombuses [33–35]; also, see Supplemental Material, Sec. A [36].

Let us first recapitulate the well-known inflation method invoked to obtain the dodecagonal tiling and its specific approximants [32,33]. To obtain the dodecagonal tiling, one starts with a cluster of 19 nodes forming a so-called “wheel” [Figs. 1(e)–1(g)]. In this cluster, all distances between the nearest nodes are the same, and we assume that they equal 1. After that, the wheel is inflated by $\tau = \sqrt{3} + 2$ times, and each of its nodes is replaced by a wheel of the original size. With this inflation coefficient, the edges

of adjacent wheels coincide exactly [Figs. 1(e)–1(g)], and the process can be continued in successive cycles. To maintain the average dodecagonal symmetry, the inserted wheels at each cycle must be randomly rotated by an angle divisible by 30° .

Similarly, by decorating the nodes of square or triangular periodic lattices with wheels and repeating n inflations, one can construct periodic approximants, which we refer to as the Stampfli approximants [32]. Note that the period of such a triangular approximant is equal to τ^n , while the period of a square one is $\sqrt{2}$ times greater, because the wheel has twofold symmetry, and in any periodic structure with fourfold symmetry, the wheel centers must be located between nearest translationally equivalent fourfold axes. We note that within the inflation approach, it is impossible to introduce the continuous phason degrees of freedom and obtain its approximants in the usual way, i.e., by a linear phason strain of the original tiling [40]. Therefore, we will first consider the growth of a quasicrystalline cluster within a model proposed below, and then modify this model by introducing phason degrees of freedom.

A. Model of condensation of quasilattice gas

Let us suppose that, during the growth of a planar cluster, a new particle can attach only at a point that is connected to at least one of the filled positions by one of the following vectors:

$$\mathbf{a}_i = \langle \cos i\pi/6, \sin i\pi/6 \rangle, \quad (1)$$

where $i = 0, 1, \dots, 11$. Note that eight of the 12 vectors \mathbf{a}_i can be expressed as integer linear combinations of the remaining basis vectors. For the sake of convenience, we use the translations with numbers 0,1,2,3 as this basis. Then, the coordinates of any filled or potentially filled position can be expressed as

$$\mathbf{r} = \sum_{i=0}^3 n_i \mathbf{a}_i, \quad (2)$$

where n_i is integers. The perpendicular coordinates \mathbf{r}^\perp of the same point is determined by the same set $\{n_i\}$, but the vectors \mathbf{a}_i are replaced by \mathbf{a}_i^\perp , where $\mathbf{a}_i^\perp = \langle \cos 5i\pi/6, \sin 5i\pi/6 \rangle$ [2]. Note that the perpendicular coordinates introduced in this way assume that there is a 4D lattice whose nodes are indexed by four integer indices, while the coordinates Eq. (2) and perpendicular coordinates are the orthogonal projections of these nodes; for more detail, see Supplemental Material, Sec. A [36].

Let the attachment of particles occur step by step. Suppose that at the current step there are q positions that can be filled by only one particle. Then we find the probability p_j of filling the j th position as

$$p_j = \exp\left(-\frac{E_j - \mu}{T}\right), \quad (3)$$

where E_j is the corresponding binding energy and the chemical potential μ determined by the expression following from the condition $\sum p_j = 1$, and T is the thermal energy. Since only one particle is necessarily attached at each step, to practically determine which of the possible positions will be filled, it is convenient to divide the interval of unit length into smaller segments with lengths proportional to the probabilities Eq. (3), and then generate a random number within the unit interval.

Note that our approach builds upon earlier works proposing that at each step of the cluster growth one of the predetermined positions is filled [41], or that the position to be filled is selected from the most energetically favorable positions around the cluster, using the Boltzmann distribution [42]. However, while our approach and the model [42] are both based on the Boltzmann distribution, the model of nonequilibrium growth of a dodecagonal cluster [31] assumes that the probability for negative values of E_j is proportional to $1 - \exp(E_j/T)$, and for positive values it is *a priori* set to zero. Since it is reasonable to assume that the binding energy E_j for any potentially occupied position is always negative, the above modification of the classical distribution function is unnecessary. In addition, our analysis shows that the dependence of the distribution on E_j/T is significantly weaker than in the case of the standard Boltzmann function. Nevertheless, in the limit $T \rightarrow 0$, both approaches naturally lead to filling the most energetically favorable positions.

In Ref. [31], the binding energy is calculated as an energy attributed to the formation of certain particle configurations. However, several years earlier and within the framework of the ordinary molecular dynamics, dodecagonal clusters were modeled using the following Lennard-Jones-Gauss (LJG) potential of pair interactions [43]:

$$V(r) = \frac{1}{r^{12}} - \frac{2}{r^6} + \epsilon \exp\left(-\frac{(r - r_0)^2}{2\sigma^2}\right). \quad (4)$$

Note that various two-minima potentials can lead to the formation of various packings [44–46]. With parameters $\epsilon = -0.866$, $\sigma = 0.02$, and $r_0 = 1.9$, the potential (4) has two separate minima at $r = 1 = |\mathbf{a}_i|$ and $r \approx 1.897 \approx |\mathbf{a}_i + \mathbf{a}_{i+1}|$ and is more suitable for assembling dodecagonal packings [47]. Note that the first minimum of the potential (4) establishes the distance between the nearest neighbors, while the second one makes it energetically advantageous to form isosceles three-particle configurations with a unit length lateral side and an apex angle of 150° . Such configurations arise when square and triangular tiles are joined. In the next section, we analyze the structures obtained within the quasilattice gas model using the potential (4) and distribution (3).

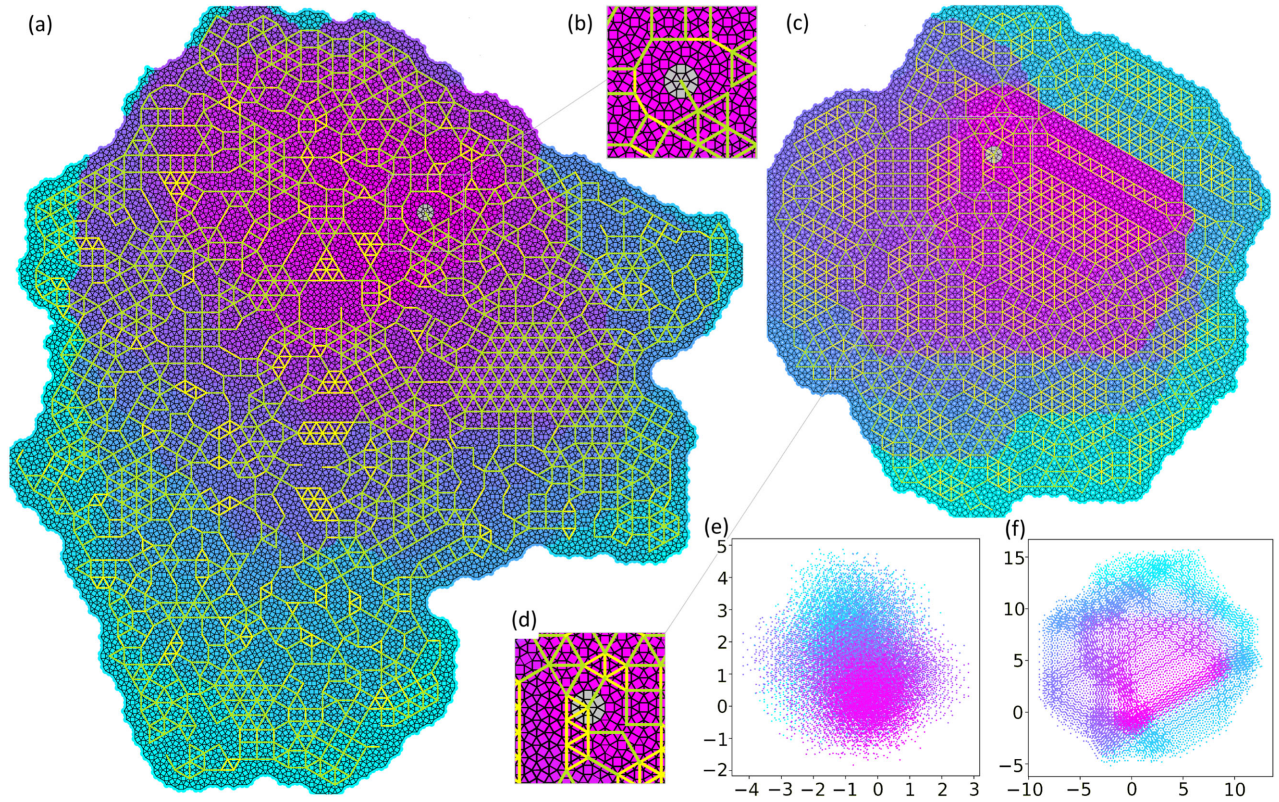


FIG. 2. Self-assembly within the quasilattice gas model at $T = 0.005$ utilizing the interaction potential (4). (a) General view of a cluster containing 20 000 particles with a morphology closer to the QC type. The change in particle color from pink to blue reflects the corresponding change in the size of the growing cluster. The initial particle is located at the center of the wheel highlighted in gray. (b) Close-up of the central part of the cluster (a). (c) General view of a cluster containing 10 000 particles whose morphology is further away from the QC type. (d) Close-up of the central part of the cluster (c). (e),(f) Perpendicular coordinates of the particles belonging to the clusters (a) and (c), respectively. In panels (a)–(d), the centers of hexagons at distances of $\sqrt{3} + 2$ and $\sqrt{3} + 1$ are connected by light green lines and yellow lines, respectively.

B. Square-triangle packings obtained with the Lennard-Jones-Gauss potential

Let us first consider the most interesting case of low temperatures, since the binding energies of proteins in their structures are often higher than the thermal energy [48,49]. Note that the calculation of occupation probabilities in the model that uses the original Boltzmann distribution is invariant with respect to the choice of the energy reference point. Therefore, in order to avoid numerical overflow, it is convenient in the region of low temperatures to first determine the position at which the attachment of a particle is more favorable energetically, and then calculate all binding energies E_j with respect to this level.

Typical results of self-assembly of planar clusters at $T = 0.005$ are presented in Fig. 2. At this temperature, structures with two types of morphology are assembled. The first type of morphology [see cluster containing 20 000 particles in Fig. 2(a)] is closer to quasicrystalline. As one can see from this figure, an aperiodic structure grows right around the origin. The corresponding area may be larger or smaller, but it is always limited. In clusters containing about 20 000

particles, as they grow, the quasicrystalline type of order smoothly turns into a periodic one, and several differently oriented triangular and square approximants emerge. They are of Stampfli type with a minimal period of $\tau = \sqrt{3} + 2$, which equals the distance between the centers of adjacent wheels; see the central part of Figs. 2(b) and 1(e)–1(g). Another interesting feature is that the approximants are disordered; i.e., the wheels are randomly rotated relative to each other. Also, there are no clear domain boundaries within the cluster. The packing consists entirely of triangular and square tiles, which sharply distinguishes this order from the structures obtained in Refs. [43,47]. Regular growth of clusters with a similar morphology can be achieved if the inflated wheel is used as an initial nucleus at least once.

The second type of morphology [see cluster containing 10 000 particles in Fig. 2(c)] is further away from quasicrystalline and corresponds to a polycrystal of smoothly conjugated square and triangular structures with a period of $\sqrt{3} + 1$. A fragment of a triangular non-Stampfli approximant [Fig. 2(d)] starts to grow directly at the cluster center. Note also that the perpendicular

projection of the set of its nodes is significantly wider, despite the 2 times smaller number of particles in the cluster; compare Figs. 2(e) and 2(f). It happens because the translations of length τ (highlighted in green) in the perpendicular space have a length of $2 - \sqrt{3}$, while the translations of length $\tau - 1$ (highlighted in yellow) in the perpendicular space correspond to a longer period of $\sqrt{3} - 1$. In addition, the portion of regions with periodic order in the second cluster is significantly higher. In the limit $T \rightarrow 0$, when the most energetically favorable positions are occupied, only the clusters with this type of morphology grow, and as we verified numerically, this always occurs at $T < 0.001$.

At higher temperatures ($T > 0.1$), the assembled clusters necessarily include extended aperiodic regions; see Supplemental Material, Fig. 2 [36]. Already at this temperature, a noticeable number of defects appears in the cluster, whose structure is represented by a random alternation of periodic approximants and aperiodic regions conjugating continuously. At $T \approx 0.2 - 0.3$, the number of defects as well as the perimeter of the cluster increase drastically. The latter is due to the fact that the boundary of the cluster is no longer smooth: Along the boundary, one can observe a number of extended fjordlike defects. In addition, multiple point defects also appear in the form of deformed hexagons and shields.

Nevertheless, it is still possible to obtain large fully S-T clusters at high temperatures if the contribution of certain three-particle interactions is taken into account. Following the idea that synthesis of dodecagonal structures requires the stabilization of triangular and square tiles [7], we assume that if the attached particle has two neighbors, the distance between which is $\sqrt{2}|\mathbf{a}_i|$ or $\sqrt{3}|\mathbf{a}_i|$, then its attachment yields an additional contribution E_3 to the binding energy. This contribution increases the probability of attaching the particle that completes a square tile or two adjacent triangular tiles. As we have verified, even at high temperatures, this two-component binding energy can lead to the tilings of exclusively S-T order.

Characterizing the obtained structures on average, we note that already at $E_3 \approx -2$, the number of fjords at the boundaries decreases sharply. As the cluster grows, they can simply disappear, turning into limited linear defects. At $E_3 \approx -3$, fjords do not appear, while extremely rare point defects may still emerge in the packings. At $E_3 < -4$ and $T \approx 0.4$, the quasicrystalline order becomes the most perfect, consisting exclusively of square and triangular tiles. Nevertheless, the perpendicular sizes of the resulting clusters turn out to be at least 2 to 3 times larger than the corresponding size of the dodecagonal Stampfli tiling [50], which indicates an essential phason disorder in the obtained structures.

For what is to follow, it is important to note that in the proposed framework, periodic approximants emerge at the $T \rightarrow 0$ limit, when the binding energy is much higher than

the thermal one. It is indeed very likely that besides the three approximants that were found, there may exist also other short-period approximants. In the next section, we pursue this line of thought and develop a phenomenological binding energy based on nD crystallography concepts. Application of this energy together with geometrical constraints resulting from the three-particle interactions, allows us to obtain all possible short-period approximants needed for the regular modeling of nanocontainers with local S-T order.

C. Effective binding energy and construction of structurally perfect square-triangle tilings

Let us consider how to construct the most structurally perfect dodecagonal S-T cluster within the framework of nonequilibrium assembly and the quasilattice gas model. Since a perfect cluster must have a minimum size in the perpendicular space, a natural way to obtain it is to put each new particle in the position with the minimum length of its perpendicular coordinate \mathbf{r}_j^\perp corresponding to the limit $T \rightarrow 0$ and the simplest effective binding energy $E_b + (\mathbf{r}_j^\perp)^2$. Here, E_b is a constant term making the energy negative; its value has no relevance at $T \rightarrow 0$. Because of its simplicity, this energy cannot prevent the attachment of particles that are too close to the occupied cluster positions (as the LJG potential does). Therefore, we must exclude them from the set of allowed positions. Additionally, we take into account the three-particle interactions introduced above: If a defective square tile or a pair of adjacent defective triangular tiles appear, we necessarily add a particle that turns these tiles into regular ones. Disabling this procedure leads to an appearance of point defects even if all other geometric constraints described below are met.

As a result of applying the above algorithm, clusters like that shown in Fig. 3(a) arise. They are indeed characterized by a radius, which is limited to one in the perpendicular space. However, the obtained structures are defective and contain symmetrical holes, the smallest of which can be perfectly filled with wheels. Therefore, it is required to impose an additional constraint on the phenomenological model.

Assuming that the cluster should grow relatively uniformly around the origin in all directions, we introduce into the model the minimum R_{\min} and maximum R_{\max} radii of the growing cluster. With each particle attached, these radii are recalculated. Let us define R_{\min} as the minimum among the lengths of \mathbf{r}_j vectors, which enumerate positions allowed for filling. Also, we suppose that the value $R_{\max} - R_{\min} = \Delta R$ is a model parameter, and at each step we will remove from the set of allowed positions all those, for which $|\mathbf{r}_j| > R_{\max}$. Clearly, the case of $\Delta R = \infty$ is identical to the simplest model discussed above.

One of the clusters obtained at $\Delta R = 0$ is shown in Fig. 3(b). The cluster structure is formed by S-T tiles and

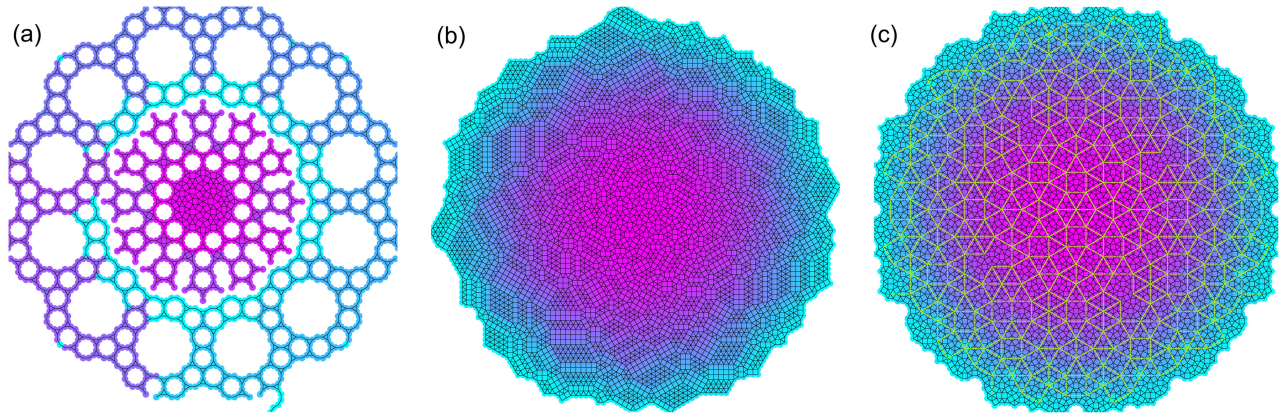


FIG. 3. Constructing the phenomenological model of square-triangle packings. (a) The simplest dodecagonal S-T packing with a minimum perpendicular size. (b) Dodecagonal S-T packing assembling under the condition $\Delta R = 0$. (c) Perfect dodecagonal S-T packing corresponding to the condition $\Delta R = 2.7$ and containing 5000 particles. A superimposed tiling (shown in light green) has edges inflated by $\tau = \sqrt{3} + 2$ times.

represents a set of smoothly conjugated regions with locally periodic orders of various types and resembles the structure shown in Fig. 2(c). The size of such clusters in perpendicular space grows infinitely with the particle number. Since the structure has no holes, it becomes clear that there is a critical value of ΔR at which holes do not yet appear, and the size of the cluster in perpendicular space is minimal. Since the smallest holes of the structure in Fig. 3(a) can be perfectly filled with wheels (whose size is $\tau = \sqrt{3} + 2$), then the critical value of ΔR should also be close to τ (and, in fact, a bit smaller than τ). Figure 3(c) in the main text and Fig. 3 in Supplemental Material [36] show the most perfect dodecagonal packings, which emerge at $\Delta R \approx 2.7$. The size of such a packing in perpendicular space [Supplemental Material, Fig. 3(b) [36]] is only slightly larger than that of the Stampfli dodecagonal tiling [50]. Accordingly, the Stampfli dodecagonal tiling has a somewhat lower total energy that can be calculated using the effective binding energy introduced in the beginning of this subsection. The diffraction patterns of both tilings are extremely similar; see Supplemental Material, Fig. 3(c) [50]. The high crystallographic perfection of the obtained tiling is also proven by the fact that the superimposed tiling of the second order (with edges inflated by τ times) contains only rare defects; see tiling in light green in Fig. 3(c).

The main advantage of the developed approach is the ability to control phason degrees of freedom of the resulting clusters. Namely, redefining the energy of particle attachment as $E_b + (\mathbf{r}_j^\perp - \hat{\mathbf{e}}\mathbf{r}_j^\parallel - \mathbf{R}_0^\perp)^2$, one can obtain clusters with various periodic structures centered at the point \mathbf{R}_0^\parallel . These structures emerge at appropriate values of 4D vector \mathbf{R}_0 and 2D tensor $\hat{\mathbf{e}}$ (see more detail in the Appendix). In the next section, we present the short-period approximants obtained in this way and use them to construct related model shells.

III. MODEL SHELLS DEDUCED FROM THE STRUCTURES OF PERIODIC APPROXIMANTS

The simplest approximants of the dodecagonal tiling are primitive square and triangular lattices. Mapping of a triangular lattice onto a sphere through icosahedron nets is well known and leads to geodesic icosahedral polyhedra. Decorating the vertices of such polyhedra with pentamers and hexamers is the base of the Caspar-Klug model [10], which describes most of the viral shells [11]. Similarly, more complex hexagonal approximants can also be mapped onto a sphere through icosahedron nets. However, the mapping of periodic structures with fourfold symmetry through the cube nets requires a more detailed consideration. First, let us note that in any planar structure with a square lattice, not all fourfold symmetry axes are equivalent; namely, between the four closest translationally equivalent axes there is a nonequivalent one. When superimposing a cube net on square order, to glue net edges smoothly, its vertices must fall on fourfold axes, which become the threefold ones of the resulting shell.

Geodesic icosahedral polyhedra and their nets are classified using two integers (h, k) , and the squared length of a distance between icosahedron vertices equals the triangulation number $T = h^2 + hk + k^2$. However, in contrast to the icosahedral case, due to the presence of nonequivalent fourfold symmetry axes, the cube nets can also be characterized by half-integer indices, and an analogous quantifier $T' = h^2 + k^2$ then takes the following values: $1/2, 1, 2, 5/2, 4, \dots$. In addition, one pair of indices can correspond to two different nets, which are obtained from each other by a shift connecting the two nearest nonequivalent fourfold symmetry axes (one in the center and one at the vertex of the unit cell). Also, we note that if the indices are half-integer, then the resulting shell does not possess fourfold symmetry axes. The simplest cubic nets ($T' \leq 4$) and the corresponding polyhedra are shown in Fig. 4.

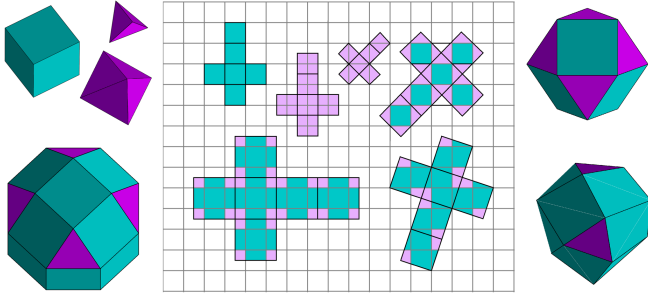


FIG. 4. The simplest cube nets ($T' \leq 4$) and the corresponding polyhedral shells. The shell vertices correspond to the nodes of the square lattice. After the net assembly, the elastic energy Eq. (5) is minimized, and the tiles in resulting polyhedra become regular or very close to regular.

If not all the polyhedron vertices are located on the symmetry axis (such examples are shown in the bottom row of Fig. 4), then to make the shell more regular, one can minimize the following elastic energy:

$$E = \sum_{i>j} (|\mathbf{r}_i - \mathbf{r}_j| - r_0)^2 + \sum_{k>l} (|\mathbf{r}_k - \mathbf{r}_l| - r'_0)^2, \quad (5)$$

where \mathbf{r}_i are the coordinates of the polyhedron vertices. The first sum in Eq. (5) runs over the edges of the polyhedron, and the second one runs over the diagonals of square tiles. The values r_0 and r'_0 are the average edge length and the average diagonal length of a square tile, respectively. After minimization of energy Eq. (5), the resulting polyhedra become either regular, i.e., consisting of regular square and triangular tiles (like in the case of rhombicuboctahedron) or the comprising tiles become very close to regular [in the case of a $(1/2, 3/2)$ polyhedron].

The vertices of all polyhedra shown in Fig. 4, except for the last one, lie on the spherical surface. The radii of the last polyhedron are characterized by their ratio of $R_{\max}/R_{\min} \approx 1.217$. Note that the radii can be equalized by retaining all the polyhedron vertices on the spherical surface during minimization of Eq. (5). Constrained and unconstrained minimizations of elastic energy are discussed in more detail below, using examples of more complex shells. For the polyhedra shown in the top row of Fig. 4, minimization of Eq. (5) is pointless since the net gluing immediately leads to the regular or semiregular polyhedra.

Let us now delve into more complex S-T structures. Figure 5 shows the first shortest-period approximants we

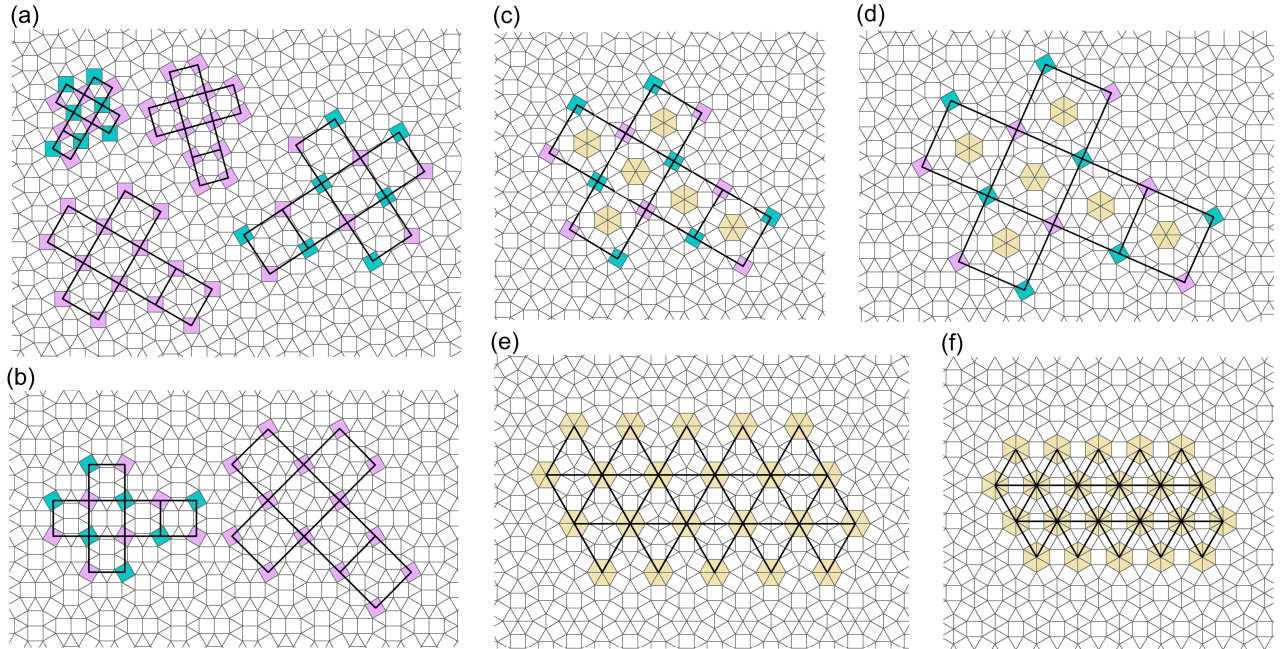


FIG. 5. First short-period approximants of the S-T dodecagonal order and the polyhedral nets corresponding to nanocontainers with octahedral, tetrahedral (a)–(d), and icosahedral (e),(f) symmetry. (a) Square approximant with the 4D translation $(1,1,0,0)$ and the period $\sqrt{2} + \sqrt{3} \approx 1.93$. In the top part of panel (a), the nets $(1/2, 1/2)$ and $(1/2, 3/2)$ with $N = 12$ and $N = 24$, respectively, are superimposed on the approximant. Below, the nets $(1,1)$ and $(1/2, 3/2)$ ($N = 48$ and $N = 60$) are shown. (b) Square approximant with the 4D translation $(1,1,1,1)$ and the period $\sqrt{6} + 3\sqrt{3} \approx 3.35$. Here, the nets $(1/2, 1/2)$ and $(1,0)$ with $N = 36$ and $N = 72$, respectively, are superimposed on the approximant. (c) Stampfli square approximant with the distance between the centers of the nearest wheels $\tau \approx 3.73$ and the net $(1/2, 1/2)$ with $N = 90$. (d) Square approximant with period $\sqrt{11 + 6\sqrt{3}} \approx 4.63$ corresponding to the 4D translation $(2,2,1,0)$. The net $(1/2, 1/2)$ with $N = 138$ is shown. (e) Triangular approximant with the 4D translation $(1,1,1,0)$ and the period $\tau - 1 \approx 2.73$. The simplest icosahedron net $N = 72$ is superimposed on the approximant. (f) Stampfli triangular approximant and the simplest icosahedron net with $N = 132$.

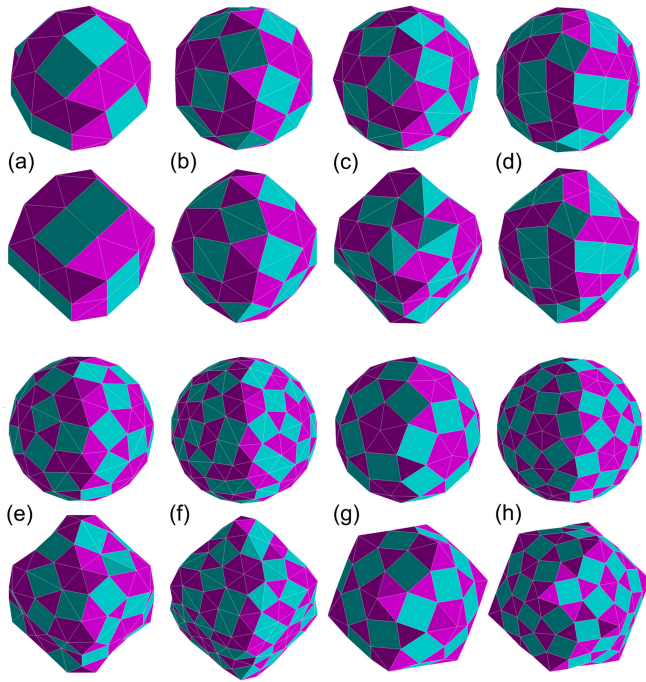


FIG. 6. Model shells with the number of vertices $N \geq 36$. (a)–(f) Structures obtained by superimposing cubic nets on square approximants. These shells have $N = 36$, $N = 48$, $N = 60$, $N = 72$, $N = 90$, and $N = 138$ vertices, respectively. (g),(h) Structures obtained by superimposing icosahedron nets on triangular approximants. The shells have $N = 72$ and $N = 132$ vertices, respectively.

have constructed. Simplest possible nets are superimposed on the approximants. In Figs. 5(a)–5(d), translationally non-equivalent fourfold axes that pass through the centers of the square tiles are highlighted in green and pink. For these cases, there is no sense in considering the shifted nets since they lead to either enantiomorphic or unchanged shells. Triangles around the sixfold symmetry axes [including the local axes in Figs. 5(a)–5(d)] are highlighted in yellow. Two of the approximants shown in Figs. 5(c) and 5(f) are Stampfli ones.

The cube net $(1/2, 1/2)$ presented in the upper left corner of Fig. 5(a) is of particular interest. Generally, after assembling the net with half-integer indices, a tetrahedral shell should appear, but in this particular case, the nodes of square order fall into the vertices of the icosahedron, and a shell with icosahedral symmetry emerges. In this context, let us emphasize that the AaLs nanocontainers discussed below are characterized by a polymorphism of icosahedral and tetrahedral structures. The assembly of the next net $(1, 0)$ shown in Fig. 5(a) leads to a snub cube structure [Fig. 1(b)], and many protein structures have a similar organization of $N = 24$ individual proteins forming a shell with the O symmetry (see the Introduction).

The rest of the model nanocontainers are shown in Fig. 6 in two versions: one with a spherical shape (in rows 1 and 3) and the other with a faceted one (in rows 2 and 4). If one supposes that $r'_0 = \sqrt{2}r_0$, then the energy minimization

makes the tiles maximally regular, and a faceting emerges. Its type (icosahedral or cubic) is determined by the type of net. Spherical polyhedra are obtained if the energy minimization is carried out under the condition that the positions of the polyhedron vertices are retained on the sphere and the relation between r_0 and r'_0 is not imposed. The latter option is more interesting since most of the real protein shells considered here are approximately spherical in shape.

Geometric parameters of the model shells shown in Fig. 6 are presented in Table I. Comparing the model shells, let us note that snub cube vertices lie exactly on the sphere; however, with an increase in N , the ratio of the maximum and minimum radii R_{\max}/R_{\min} for faceted model structures also increases. Nevertheless, among the shells presented in Table I, faceted polyhedra with O symmetry (obtained through a cube net) have smaller ratios R_{\max}/R_{\min} than polyhedra with icosahedral symmetry. The degree of regularity of triangular and square tiles in faceted and spherical shells can be introduced as the standard deviations Δ and Δ' of the values r_0/R_{\min} and r'_0/R_{\min} (Table I). In particular, both faceted icosahedral shells and a cubic shell with T_h symmetry ($N = 36$) consist of only regular triangular and square tiles.

Correspondingly, Δ and Δ' as well as the energy Eq. (5) of these shells are equal to zero (the first and last two columns of Table I). For the same structures but with a spherical shape, the presence of corresponding mirror reflection planes results in equal diagonals of all square tiles and $\Delta' = 0$. For other shells with $N \geq 60$ obtained through a cube net, the values of Δ and Δ' in the faceted versions of the polyhedra are 5 to 10 times smaller than in the spherical versions.

In future studies, a more detailed theory based on the above results can be developed, precisizing how the shells with S-T order change their shape depending on the relationship between bending and the in-plane rigidities of the shell. Such a theory would be a generalization of both the present study and the theory [51] that shows how the relationship between mechanical parameters controls the shape of the icosahedral shells built from identical triangular finite elements. Following Ref. [52], one can also consider an additional generalization elucidating the effect of protein charges on the shape of the shells with quasicrystalline local order.

IV. EXPERIMENTALLY OBSERVED SHELLS WITH A SQUARE-TRIANGULAR ORDER

In the general case, the placement of structural units at vertices of model polyhedra is accompanied by vertex displacements and can lead to the polyhedron symmetry breaking. The vertex does not shift if and only if the global symmetry axis of the polyhedron passes through this vertex, and its local symmetry is compatible with that of the structural unit.

The polyhedra shown in Fig. 4 correspond to the simplest square approximant. However, after gluing the cubic nets,

TABLE I. Geometric parameters of model nanocontainers. The first row shows the number of vertices N in the shell and its symmetry. The value of N allows us to unambiguously correlate the columns of the table with the nets shown in Fig. 5.

	$N = 36, T_h$	$N = 48, O$	$N = 60, T$	$N = 72, O$	$N = 90, T$	$N = 138, T$	$N = 72, I_h$	$N = 132, I_h$
R_{\max}/R_{\min}	1.228 53	1.121 44	1.230 39	1.145 76	1.280 34	1.357 14	1.160 04	1.19 260
Faceted $r_0/R_{\min} \pm \Delta$	0.713 64 \pm 0	0.561 89 \pm 0.010 24	0.539 33 \pm 0.002 25	0.458 46 \pm 0.006 64	0.454 03 \pm 0.000 29	0.376 88 \pm 0.005 32	0.447 83 \pm 0	0.336 77 \pm 0
shells $r'_0/R_{\min} \pm \Delta'$	1.009 24 \pm 0	0.794 62 \pm 0.012 94	0.762 73 \pm 0.002 66	0.648 36 \pm 0.007 22	0.642 09 \pm 0.000 31	0.552 99 \pm 0.006 24	0.633 34 \pm 0	0.476 26 \pm 0
Round $r_0/R_{\min} \pm \Delta$	0.608 67 \pm 0.039 89	0.526 52 \pm 0.039 54	0.472 06 \pm 0.050 02	0.431 21 \pm 0.048 29	0.387 19 \pm 0.055 85	0.379 \pm 0.062 72	0.429 35 \pm 0.057 62	0.318 80 \pm 0.055 41
shells $r'_0/R_{\min} \pm \Delta'$	0.866 07 \pm 0	0.759 85 \pm 0.049 14	0.675 24 \pm 0.024 75	0.615 93 \pm 0.052 61	0.552 21 \pm 0.033 67	0.445 49 \pm 0.037 06	0.629 34 \pm 0	0.457 02 \pm 0

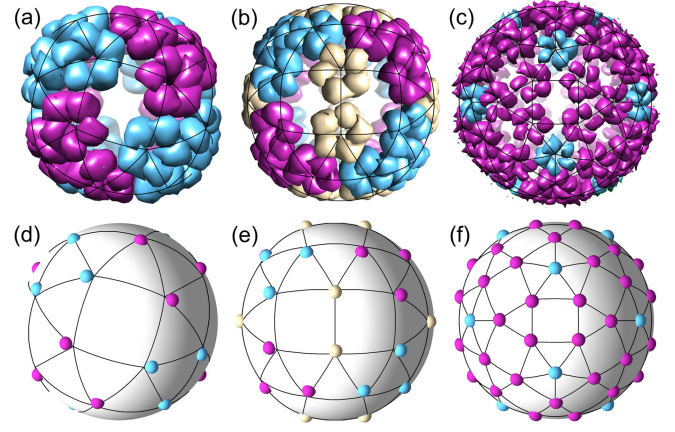


FIG. 7. Structures of AaLs nanocontainers and spherical polyhedra with S-T order superimposed on their surfaces. (a)–(c) Nanocontainers 7A4F, 7A4G, and 5MQ7, respectively. (d)–(f) Spherical model shells. Positions of small balls correspond to the centers of pentamers. The procedure for calculating the coordinates of the spherical polyhedron vertices is described in the text.

triangular tiles may appear in the resulting structures. Such nanoclusters are widely observed in nature. Along with the proteinaceous complex shown in Fig. 1(c), many other structurally analogous metallic and metal-organic clusters are known (see, for example, Ref. [53]).

We next move on to shells based on other approximants. Let us discuss approximately spherical AaLs nanocontainers formed from pentamers. Depending on mutations in the initial proteins [29,30], the shells take on one of four structures with tetrahedral or icosahedral symmetries (Fig. 7). The simplest structure includes 12 pentamers located at the vertices of an icosahedron [54]. Recall that this polyhedron can be obtained using either the simplest triangular approximant or the first nontrivial square one; see the net (1/2, 1/2) in Figs. 5(a) and 7(a). Note also that pentamer placing reduces the symmetry of the decorated shell I_h down to I .

The shells, in which individual proteins are located at the vertices of a snub cube, were presented in the Introduction. In these shells, the proteins are symmetrically equivalent, the shell has O symmetry, and the difference between positions of the mass centers of individual proteins and vertices of the snub cube is minimal. In contrast, placing pentamers at the vertices of the snub cube reduces the symmetry from O to T , and induces a small shift of the pentamer centers away from the vertices of the snub cube because the pentamers cannot form four equivalent bonds along the edges of the square. They chose their orientation in such a way that their contacts are localized only along the two opposite edges of the square [55]. As a result, in this nanocontainer the fourfold axis disappears while two types of symmetrically nonequivalent pentamers appear; see Fig. 7(a).

Figure 7(b) compares the structure of a spherical polyhedron with T_h symmetry, which has 36 vertices, with the

structure of the corresponding AaLs nanocontainer. The placement of pentamers leads to a $T_h \rightarrow T$ symmetry breaking and the splitting of the two orbits of the polyhedron vertices into three orbits of the pentamer centers. Finally, Fig. 7(c) shows the last example, comparing the shell consisting of 72 AaLs pentamers and corresponding spherical polyhedron [earlier shown in Fig. 6(g)].

All experimentally known AaLs nanocontainers have the same motif of bonds between pentamers, which have the form of a flattened hexagon. The centers of the pentamers closest to the center of the flattened hexagon form an approximate square, but only the pentamers lying along the perimeter of the hexagon are in contact with each other [29]. On a plane, the internal angles of the flattened hexagon (formed by a square and two triangular tiles) are equal to 60° or 150° . Spherical AaLs nanocontainers are designed so that the first angle can be slightly increased, while the second can be decreased, which facilitates the establishment of bonds between pentamers. In Ref. [55], an attempt was made to predict other spherical shells with the same motif of bonds between pentamers. Having considered possible packings of flattened hexagons, they concluded that two additional tetrahedral shells of 48 and 60 pentamers are possible, and our analysis shows that these shells correspond to the polyhedra shown in Figs. 6(b) and 6(c).

We have tried to superimpose the motif of flattened hexagons on other polyhedra, noting that while it can be done locally, the resulting shells have holes, and it is likely that such shells cannot be assembled from AaLs pentamers but can be assembled from other structural units. For example, using the spherical polyhedron shown in Fig. 6(h) [which originates from the Stampfli approximant presented in Fig. 5(f)], one can rationalize viral shells from the *Partitiviridae* and *Picobirnaviridae* families (Fig. 8). Such shells consist of 120 proteins, whereas the model shell has 12 additional positions lying on the icosahedron symmetry axes. These positions cannot be occupied by the asymmetric proteins and thus remain empty [Fig. 8(b)] [56].

Antigen-displaying nanoparticles I53_dn5 (6VFJ) composed of artificial proteins have an analogous structure [57]. Their proteins, like AaLs pentamers, can form other polymorphic shells with octahedral and tetrahedral symmetry [57], which are further discussed at the end of this section.

Also, we note that the shells shown in Figs. 6(g) and 6(h) and consisting of tetrahedral SUs appear on the surface of a growing icosahedral quasicrystalline cluster when the cluster is formed from an undercooled liquid [58].

Let us proceed to two examples of shells with QC local order and cubic nets. Figure 8(c) shows a nanocontainer consisting of 48 individual proteins, which has O symmetry [59]. Although in this shell, only tiles lying on the fourfold and threefold axes of the O symmetry group have fully regular shape. A comparison of the protein mass centers with the positions of the nodes of the model

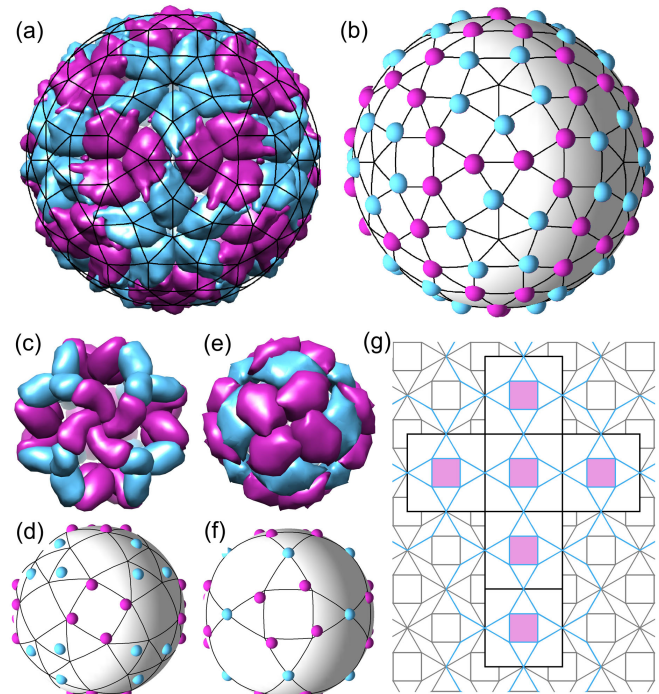


FIG. 8. Proteinaceous shells in which individual proteins form square-triangular local order. (a),(b) Capsid of human picobirnavirus (6Z8D) and its model. Centers of small balls are the mass centers of individual proteins in the shell. Black lines show the icosahedral spherical polyhedron with 132 vertices. (c),(d) Nanocontainer consisting of 48 proteins (8FWD) and the protein mass centers. (e) Shell consisting of 36 MS2 dimers (2VTU). (f) Mass centers of the dimers in the shell (e). (g) Square net of the shell (f). Outside of the net, tiling is completed by the addition of square and rhombic tiles.

spherical shell reveals that the experimentally observed structure agrees well with our theoretical framework; see Figs. 8(d) and 6(b).

Dimers forming the icosahedral capsid of bacteriophage MS2 [60] can also self-assemble into a cubic shell with O symmetry [Fig. 8(e)]. To unveil the underlying spherical tiling, we calculated the positions of mass centers of all 36 dimers in this shell and then connected them based on the dimer-dimer contacts in the real structure. After that, by minimizing elastic energy Eq. (5) corresponding to the tiling, we obtained the positions of the nodes of the resulting model shell. As can be seen in Fig. 9(d), the differences between their position and positions of dimer mass centers in the real structure are very small. At the same time, S-T order on the sphere surface is defective: The centers of the hexagons lying around threefold symmetry axes remain empty. This is due to the fact that dimers have twofold symmetry and thus cannot occupy positions on threefold axes [56,61]. In Fig. 8(g), the net of the obtained spherical structure is shown with blue lines. The underlying approximant has the same period as the one shown in Fig. 5(a), although the way in which it is decorated with square and triangular tiles is different.

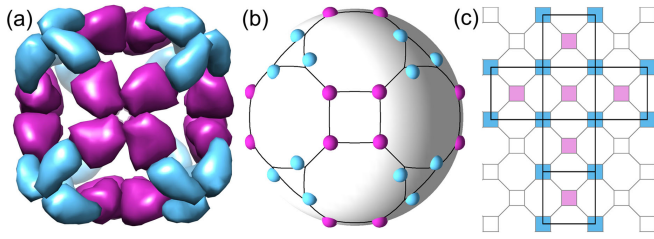


FIG. 9. A shell with octagonal local order. (a) Octahedral nanoparticle 6VFI formed from 48 proteins. (b) Corresponding model shell. Centers of small balls are the projections of protein mass centers on the spherical surface. (c) Periodic tiling consisting of squares and octagons with cubic net (1,1) on top.

Also note that in order to tile empty regions around fourfold axes (that turn into threefold axes in the shell) one must use 30° rhombs. In Fig. 8(g), outside of the net, the tiling is completed with additional squares and rhombs. This approximant can be assembled in the framework of the lattice gas condensation model, provided that the phenomenological binding energy is minimized without additional constraints on the set of allowed positions (see Sec. II C).

Concluding this section, we note that shells with square and triangular tiles in their structure can originate not only from dodecagonal but also from octagonal approximants. Figure 9(a) shows antigen-displaying nanoparticles O43_dn18, which have the O symmetry and consist of 48 artificial proteins [57]. The shell has a visible cubic faceting and empty octagons in the structure. Figure 9(b) shows the spherical model shell consisting of triangles, squares, and octagons and projections of protein mass centers on the spherical surface. When constructing this shell, the edges of the spherical tiling were equalized by minimizing energy Eq. (5). Figure 9(c) demonstrates parent periodic tiling consisting of squares and octagons with cubic net (1,1) on top.

Interestingly, there is a tetragonal antigen-displaying nanoparticle T33_dn10 [57], which assembles from the same proteins, and corresponds to net (1,0) superimposed on the same periodic motif. Thus, at least a dozen shells, where protein order corresponds to the structures of short-period quasicrystalline approximants, is already known, and it is safe to assume that in the near future even more such shells will be discovered. We hope that the theory developed in this work will help in the search for analogous nanocontainers that may play an important role in various fields of nanotechnology and nanomedicine.

V. DISCUSSION AND CONCLUSION

In recent years, protein nanoparticles and nanoshells with unconventional structural organization have begun to be synthesized and used for various practical applications in nano- and medical sciences. These protein assemblies are fundamentally different from the ones typically observed in icosahedral viral capsids, and, as we showed

above, some of the unconventional shells share common structural organization motifs with planar quasicrystals. Examining hundreds of structures from PDB, we identified a whole series of such protein shells based upon the S-T order and containing up to 360 individual proteins. The S-T order is the most common type of quasicrystalline order possible in soft-matter systems, and it is not surprising that we found a number of protein shells displaying similar structural organization that originates from short-period approximants of dodecagonal and octagonal quasicrystalline tilings. Triangular tiles in shells of the latter type appear exclusively on threefold axes as topological defects associated with the transfer of octagonal order to the sphere.

After an exhaustive search, we were unable to identify any published method for a regular construction of periodic approximants with an S-T order, and we therefore developed our own methodology as a part of this study. We proposed a new model describing the nonequilibrium growth of an S-T cluster with desired periodicity, with the probability of a particle attachment to the cluster in a certain position calculated from the Boltzmann distribution dependent on the temperature and the corresponding binding energy. After considering the traditional microscopic two-minimum potential Eq. (4) to calculate the binding energy, we elaborated a more straightforward phenomenological approach, within which the binding energy explicitly depends on the 4D coordinates of the quasilattice positions and the macroscopic 4D shift vector. Subsequently, in the framework of the traditional phason strain approach, we obtained all possible short-period dodecagonal approximants with S-T order and used them to construct icosahedral and cubic nets of the polyhedral model shells. It is interesting to note that in order to classify the cubic nets, one needs to invoke the half-integer indices along with the integer ones. After folding the nets and gluing their edges together, we obtained the polyhedra and then minimized their energy Eq. (5) to make the quasicrystalline order more regular. For this regularization, we considered two different options, leading to faceted and more typical spherical shapes observed in real shells. Note that small icosahedral capsids (containing up to 360 proteins) are also almost spherical in most cases.

The theory that we developed successfully reproduces all the shells with the S-T order that we found in the PDB, and establishes new general rules that control the structure of such shells; it is significant that the proposed theory predicts yet undiscovered analogous shells [Figs. 6(c), 6(e), and 6(f)].

Some limitations of our approach may be related to the fact that all the shells found were able to be rationalized within the framework of linear periodic approximants and regular nets of icosahedron and cube types. Nevertheless, the phason strain can be nonlinear, and the nets can be asymmetric, possibly guiding a more general approach.

Discussing the general reasons that can lead to the formation of protein shells with the S-T order, we first

note that even protein numbers in these assemblies are not compatible with the paradigmatic CK model [10], which describes the majority of known protein shells. However, the CK principle of quasiequivalence (according to which the proteins strive to form a minimum number of equivalent or quasiequivalent bonds with their neighbors) itself still continues to work, and the formation of symmetrical shells with regular nets allows proteins to minimize the number of their environments.

The CK model is also violated by some small icosahedral capsids exhibiting a protein order which is in no way similar to the square-triangular one [15,16,56]. In both cases, the restrictions imposed by the symmetry on the possible number of structural units in a shell and the connection between the intrinsic curvature of the structural units and the shell radius lead to specific ways of protein organizations. When the intrinsic curvature of structural units tends to zero, it ceases to influence the radius and, as a consequence, the number of proteins in the shell. Therefore, spherical shells that violate the CK model become extremely rare.

Discussing a possible mechanism for the assembly of shells with the S-T local order, we stress that, as we found, planar S-T periodic approximants readily assemble within the framework of a nonequilibrium assembly model when $T \rightarrow 0$, and attachment of the next structural unit occurs in one of the most energetically favorable positions near the growing cluster. It is therefore likely that a similar nonequilibrium assembly mechanism could operate for both spherical shells with S-T order and some other protein structures, reducing the likelihood of their misassembly. In this context, it is worth recalling the very-high-temperature stability of AaLs nanocontainers [29], which clearly means that under normal conditions the binding energy of pentamers in this system is significantly greater than the thermal energy.

In future studies, it would be interesting to obtain the quasicrystalline shells also in the framework of approaches that are based either on the minimization of energy or on an appropriate cost function [62]. In particular, it is worth considering the nonequilibrium assembly of particles confined to a spherical substrate and interacting via a suitable potential. Since in the case of nonequilibrium assembly the planar dodecagonal approximants emerge at $T \rightarrow 0$, we suggest that spherical shells with analogous quasicrystalline order can be formed in the same limit, provided an appropriate choice is made for the double-minimum potential and the substrate radius. As a side note, we emphasize that due to the substrate curvature the second minimum of the potential should be relatively closer to the origin than in the planar case. It is also worth noting that some of the simplest S-T packings on a spherical surface can be obtained by using a single-minimum Lennard-Jones potential. By attaching particles to the most energetically favorable positions near the growing spherical cluster

and minimizing the cluster energy after each attachment, we obtained the snub cube, cuboctahedron, and rhombicuboctahedron structures, together with several other shells with S-T order as well as various geodesic polyhedra with icosahedral symmetry. We leave the many details of the nonequilibrium assembly of the spherical shells to a future study.

It is worth noting that the methods developed in this paper can be also applied in the theory of ordinary quasicrystals. The model of quasilattice gas condensation combined with the proposed phenomenological binding energy allows us to construct, not only the linear S-T approximants, but also structurally perfect dodecagonal S-T tilings which, while being morphologically close to the Stampfli tiling, differ from each other by a homogeneous phason shift. Our approach that introduces and operates with macroscopic phason degrees of freedom of dodecagonal S-T packings can be of great use for the development of various physical and structural models of systems exhibiting this type of order, which is quite widespread both in soft matter as well as in metal alloys.

Finally, the structural relationships between spherical proteinaceous shells and planar quasicrystals are potentially important because quasicrystals have material properties that are starkly different from those of crystals. Thus, our study may be of interest not only to specialists dealing with the development of design and applications of various proteinaceous nanocontainers, but also to a wide range of readers interested in chemistry and physics of condensed matter, as well as modern problems of nD crystallography.

ACKNOWLEDGMENTS

S. R. and O. K. acknowledge financial support from the Russian Science Foundation, Grant No. 22-12-00105. R. P. acknowledges funding from the Key Project No. 12034019 of the Natural Science Foundation of China.

S. R. proposed the main approaches. A. R. modeled planar quasicrystals. O. K. found examples of appropriate proteinaceous shells and together with A. R. drew the figures. A. R. and O. K. carried out the numerical simulations. S. R. with the essential help of R. P. wrote the draft. All authors contributed to the final version of this manuscript. All authors have approved the final version.

APPENDIX: CONSTRUCTION OF PERIODIC APPROXIMANTS WITH SQUARE AND TRIANGULAR LATTICES

First, let us note that one can uniformly shift the cluster by a 4D translation vector \mathbf{T}_0 . To obtain a shifted packing, one should impose a condition on the minimum lengths of the vectors $\mathbf{r}_j^\perp - \mathbf{T}_0^\perp$ instead of the vectors \mathbf{r}_j^\perp , and the packing should be assembled around the point with coordinates \mathbf{T}_0^\parallel , instead of the origin. Because of the

presence of 4D translation symmetry in the model, the packing shifted by the 4D translation turns out to be simply shifted by its parallel component. In a more general case of an arbitrary 4D shift vector \mathbf{R}_0 , along with a shift of the cluster center, a phason rearrangement of the structure also occurs; see Supplemental Material, Figs. 3(d) and 3(e) [36].

The next step in obtaining approximants is the introduction of phason strain into the model. To do so, when constructing a cluster and choosing a position to be filled, along with considering the displacement of cluster center, one must require the length $|\mathbf{r}_j^\perp - \mathbf{f}_j^\perp|$ to be minimal. In this expression, \mathbf{f}_j^\perp is a function of \mathbf{r}_j^\parallel that describes the phason strain. Accordingly, the energy of particle attachment must be redefined as $E_b + (\mathbf{r}_j^\perp - \mathbf{f}_j^\perp)^2$. To construct linear approximants, we suppose that $\mathbf{f}_j^\perp = \mathbf{R}_0^\perp + \hat{\mathbf{e}}\mathbf{r}_j^\parallel$, where $\hat{\mathbf{e}}$ is a constant tensor of the linear phason strain. This approach allows us to regularly obtain periodic S-T approximants, including those that are different from the Stampfli ones.

The shells considered in this work are based on cubic and icosahedral nets. Thus, we need to construct the approximants with square and triangular lattices only. The construction of these approximants starts with the selection of components $\{n_i\}$ of the first 4D translation \mathbf{A}_1 . In order to reduce the enumeration of possible 4D translations, we assume that the direction of the parallel component \mathbf{A}_1^\parallel is limited to the 30° sector, and its length is less than 5 (since we consider short-period approximants only). We also assume that the length of the orthogonal projection \mathbf{A}_1^\perp is smaller than the maximal radius (approximately 1.3) of the Stampfli tiling in the perpendicular space.

By rotating translation \mathbf{A}_1 by 60° or 90° , one can find the second 4D translation \mathbf{A}_2 of the considered approximant. In fact, to get the explicit forms of components \mathbf{A}_2^\parallel and \mathbf{A}_2^\perp , one needs to replace index i in the expressions for \mathbf{a}_i and \mathbf{a}_i^\perp . A 60° rotation corresponds to the replacement $i \rightarrow i + 2$, while a 90° rotation corresponds to $i \rightarrow i + 3$. Then, using the obtained components, we calculate linear phason strain tensor \mathbf{e} , whose coefficients are expressed through standard relations $\mathbf{A}_1^\perp = \hat{\mathbf{e}}\mathbf{A}_1^\parallel$ and $\mathbf{A}_2^\perp = \hat{\mathbf{e}}\mathbf{A}_2^\parallel$.

Since approximants with square lattices are assembled around a central square tile, one must use an appropriate homogeneous 4D shift \mathbf{r}_0 upon their generation. In the special case when the edges of this square tile are parallel to vectors \mathbf{a}_0 and \mathbf{a}_3 , \mathbf{R}_0 equals $(1, 0, 0, 1)/2$. For other possible orientations of the central tile 4D vector, \mathbf{R}_0 can be found analogously. Approximants with triangular lattices are constructed around a central particle; thus, for them $\mathbf{R}_0 = 0$.

Regarding the limitations of this method, we first note that periodic S-T order is not compatible with all possible \mathbf{A}_1 and \mathbf{A}_2 vector pairs. In the case of incompatibility, instead of exact translations, \mathbf{A}_1^\parallel and \mathbf{A}_2^\parallel refer to average

translations. Second, even if it is possible to construct a periodic approximant using these translations, the wheels (if they exist in the structure) turn out to be randomly oriented.

-
- [1] D. Shechtman, I. Blech, D. Gratias, and J. W. Cahn, *Metallic phase with long-range orientational order and no translational symmetry*, *Phys. Rev. Lett.* **53**, 1951 (1984).
 - [2] W. Steurer, *Twenty years of structure research on quasicrystals. Part I. Pentagonal, octagonal, decagonal and dodecagonal quasicrystals*, *Z. Kristallogr.* **219**, 391 (2004).
 - [3] X. Zeng, G. Ungar, Y. Liu, V. Percec, A. E. Dulcey, and J. K. Hobbs, *Supramolecular dendritic liquid quasicrystals*, *Nature (London)* **428**, 157 (2004).
 - [4] X. Ye, J. Chen, M. Eric Irrgang, M. Engel, A. Dong, S. C. Glotzer, and C. B. Murray, *Quasicrystalline nanocrystal superlattice with partial matching rules*, *Nat. Mater.* **16**, 214 (2017).
 - [5] T. M. Gillard, S. Lee, and F. S. Bates, *Dodecagonal quasicrystalline order in a diblock copolymer melt*, *Proc. Natl. Acad. Sci. U.S.A.* **113**, 5167 (2016).
 - [6] K. Hayashida, T. Dotera, A. Takano, and Y. Matsushita, *Polymeric quasicrystal: Mesoscopic quasicrystalline tiling in ABC star polymers*, *Phys. Rev. Lett.* **98**, 195502 (2007).
 - [7] T. Ishimasa, *Dodecagonal quasicrystals still in progress*, *Isr. J. Chem.* **51**, 1216 (2011).
 - [8] A. Jayaraman, C. M. Baez-Cotto, T. J. Mann, and M. K. Mahanthappa, *Dodecagonal quasicrystals of oil-swollen ionic surfactant micelles*, *Proc. Natl. Acad. Sci. U.S.A.* **118**, e2101598118 (2021).
 - [9] T. Dotera, T. Oshiro, and P. Ziherl, *Mosaic two-lengthscale quasicrystals*, *Nature (London)* **506**, 208 (2014).
 - [10] D. L. D. Caspar and A. Klug, *Physical principles in the construction of regular viruses*, *Cold Spring Harbor Symp. Quant. Biol.* **27**, 1 (1962).
 - [11] R. Zandi, B. Dagnea, A. Travesset, and R. Podgornik, *On virus growth and form*, *Phys. Rep.* **847**, 1 (2020).
 - [12] O. V. Konevtsova, D. V. Chalin, and S. B. Rochal, *Theory of density waves and organization of proteins in icosahedral virus capsids*, *Phys. Chem. Chem. Phys.* **26**, 569 (2024).
 - [13] R. Twarock, *A tiling approach to virus capsid assembly explaining a structural puzzle in virology*, *J. Theor. Biol.* **226**, 477 (2004).
 - [14] R. Twarock and A. Luque, *Structural puzzles in virology solved with an overarching icosahedral design principle*, *Nat. Commun.* **10**, 4414 (2019).
 - [15] O. V. Konevtsova, S. B. Rochal, and V. L. Lorman, *Chiral quasicrystalline order and dodecahedral geometry in exceptional families of viruses*, *Phys. Rev. Lett.* **108**, 038102 (2012).
 - [16] O. V. Konevtsova, V. V. Pimonov, V. L. Lorman, and S. B. Rochal, *Quasicrystalline and crystalline types of local protein order in capsids of small viruses*, *J. Phys. Condens. Matter* **29**, 284002 (2017).
 - [17] J. E. Johnson, *Functional implications of protein-protein interactions in icosahedral viruses*, *Proc. Natl. Acad. Sci. U.S.A.* **93**, 27 (1996).

- [18] T. Dotera, *Quasicrystals in soft matter*, *Isr. J. Chem.* **51**, 1197 (2011).
- [19] H. M. Berman, J. Westbrook, Z. Feng, G. Gilliland, T. N. Bhat, H. Weissig, I. N. Shindyalov, and P. E. Bourne, *The Protein Data Bank*, *Nucleic Acids Res.* **28**, 235 (2000).
- [20] T. G. Laughlin *et al.*, *Architecture and self-assembly of the jumbo bacteriophage nuclear shell*, *Nature (London)* **608**, 429 (2022).
- [21] L. Cappadocia, A. Marechal, J. S. Parent, E. Lepage, J. Sygusch, and N. Brisson, *Crystal structures of DNA-Whirly complexes and their role in Arabidopsis organelle genome repair*, *Plant Cell* **22**, 1849 (2010).
- [22] M. Li, Z. Chen, P. Zhang, X. Pan, C. Jiang, X. An, S. Liu, and W. Chang, *Crystal structure studies on sulfur oxygenase reductase from Acidianus tengchongensis*, *Biochem. Biophys. Res. Commun.* **369**, 919 (2008).
- [23] S. E. Glynn *et al.*, *Structure and mechanism of imidazoleglycerol-phosphate dehydratase*, *Structure* **13**, 1809 (2005).
- [24] L. Toussaint, L. Bertrand, L. Hue, R. R. Crichton, and J. P. Declercq, *High-resolution x-ray structures of human apo-ferritin H-chain mutants correlated with their activity and metal-binding sites*, *J. Mol. Biol.* **365**, 440 (2007).
- [25] G. Petruk, D. M. Monti, G. Ferraro, A. Pica, L. D'Elia, F. Pane, A. Amoresano, J. Furrer, K. Kowalski, and A. Merlino, *Encapsulation of the dinuclear trithiolato-bridged arene ruthenium complex diruthenium-1 in an apoferritin nanocage: Structure and cytotoxicity*, *ChemMedChem* **14**, 594 (2019).
- [26] W. Ranatunga, O. Gakh, B. K. Galeano, D. Y. Smith IV, C. A. Soderberg, S. Al-Karadaghi, J. R. Thompson, and G. Isaya, *Architecture of the yeast mitochondrial iron-sulfur cluster assembly machinery: The sub-complex formed by the iron donor, Yfh1, and the scaffold, Isu1*, *J. Biol. Chem.* **291**, 10378 (2016).
- [27] W. Aeschmann, S. Kammer, S. Staats, P. Schneider, G. Schneider, G. Rimbach, M. Cascella, and A. Stocker, *Engineering of a functional gamma-tocopherol transfer protein*, *Redox Biol.* **38**, 101773 (2021).
- [28] T. Krojer, J. Sawa, E. Schäfer, H. R. Saibil, M. Ehrmann, and T. Clausen, *Structural basis for the regulated protease and chaperone function of DegP*, *Nature (London)* **453**, 885 (2008).
- [29] E. Sasaki, D. Bohringer, M. van de Waterbeemd, M. Leibundgut, R. Zschoche, A. J. Heck, N. Ban, and D. Hilvert, *Structure and assembly of scalable porous protein cages*, *Nat. Commun.* **8**, 14663 (2017).
- [30] S. Tetter *et al.*, *Evolution of a virus-like architecture and packaging mechanism in a repurposed bacterial protein*, *Science* **372**, 1220 (2021).
- [31] C. Xiao, N. Fujita, K. Miyasaka, Y. Sakamoto, and O. Terasaki, *Dodecagonal tiling in mesoporous silica*, *Nature (London)* **487**, 349 (2012).
- [32] P. A. Stampfli, *Dodecagonal quasi-periodic lattice in two dimensions*, *Helv. Phys. Acta.* **59**, 1260 (1986), <https://www.e-periodica.ch/cntmng?pid=hpa-001%3A1986%3A59%3A%3A1521>.
- [33] M. Oxborrow and C. L. Henley, *Random square-triangle tilings: A model for twelvefold-symmetric quasicrystals*, *Phys. Rev. B* **48**, 6966 (1993).
- [34] F. Gähler, *Crystallography of dodecagonal quasicrystals, in Quasicrystalline Materials*, edited by C. Janot and J. M. Dubois (World Scientific, Singapore, 1988), pp. 272–284.
- [35] P. W. Leung, C. L. Henley, and G. V. Chester, *Dodecagonal order in a two-dimensional Lennard-Jones system*, *Phys. Rev. B* **39**, 446 (1989).
- [36] See Supplemental Material at <http://link.aps.org/supplemental/10.1103/PhysRevX.14.031019> for additional notes and figures, which includes Refs. [37–39].
- [37] P. Bak, *Phenomenological theory of icosahedral incommensurate (“quasiperiodic”) order in Mn-Al alloys*, *Phys. Rev. Lett.* **54**, 1517 (1985).
- [38] P. Bak, *Symmetry, stability, and elastic properties of icosahedral incommensurate crystals*, *Phys. Rev. B* **32**, 5764 (1985).
- [39] S. B. Rochal and Y. A. Kozinkina, *Theory of the defect-free phason strain in quasicrystals*, *Phys. Rev. B* **72**, 024210 (2005).
- [40] W. Steurer and S. Deloudi, *Crystallography of Quasicrystals: Concepts, Methods and Structures* (Springer-Verlag, Berlin, 2009).
- [41] D. J. Wales, *Closed-shell structures and the building game*, *Chem. Phys. Lett.* **141**, 478 (1987).
- [42] F. Baletto, A. Rapallo, G. Rossi, and R. Ferrando, *Dynamical effects in the formation of magic cluster structures*, *Phys. Rev. B* **69**, 235421 (2004).
- [43] M. Engel and H. R. Trebin, *Self-assembly of monatomic complex crystals and quasicrystals with a double-well interaction potential*, *Phys. Rev. Lett.* **98**, 225505 (2007).
- [44] M. Dzugutov, *Glass formation in a simple monatomic liquid with icosahedral inherent local order*, *Phys. Rev. A* **46**, R2984 (1992).
- [45] M. Dzugutov, *Monatomic model of icosahedrally ordered metallic glass formers*, *J. Non-Cryst. Solids* **156–158**, 173 (1993).
- [46] J. P. K. Doye, D. J. Wales, F. H. M. Zetterling, and M. Dzugutov, *The favored cluster structures of model glass formers*, *J. Chem. Phys.* **118**, 2792 (2003).
- [47] J. H. Chen, C. Cai, and X. J. Fu, *Decagonal and dodecagonal quasicrystals obtained by molecular dynamics simulations*, *Chin. Phys. Lett.* **36**, 036101 (2019).
- [48] T. Clackson and J. A. Wells, *A hot spot of binding energy in a hormone-receptor interface*, *Science* **267**, 383 (1995).
- [49] C. Chothia and J. Janin, *Principles of protein–protein recognition*, *Nature (London)* **256**, 705 (1975).
- [50] M. Baake, R. Klitzing, and M. Schlottman, *Fractally shaped acceptance domains of quasiperiodic square-triangle tilings with dedecagonal symmetry*, *Physica (Amsterdam)* **191A**, 554 (1992).
- [51] J. Lidmar, L. Mirny, and D. R. Nelson, *Virus shapes and buckling transitions in spherical shells*, *Phys. Rev. E* **68**, 051910 (2003).
- [52] D. Roshal, O. Konevtsova, A. Lošdorfer Božič, R. Podgornik, and S. Rochal, *pH-induced morphological changes of proteinaceous viral shells*, *Sci. Rep.* **9**, 5341 (2019).
- [53] X. Ma, Y. Bai, Y. Song, Q. Li, Y. Lv, H. Zhang, H. Yu, and M. Zhu, *Rhombicuboctahedral Ag₁₀₀: Four-layered octahedral silver nanocluster adopting the Russian nesting*

- doll model*, *Angew. Chem., Int. Ed. Engl.* **59**, 17234 (2020).
- [54] X. Zhang, W. Meining, M. Fischer, A. Bacher, and R. Ladenstein, *X-ray structure analysis and crystallographic refinement of lumazine synthase from the hyperthermophile Aquifex aeolicus at 1.6 Å resolution: Determinants of thermostability revealed from structural comparisons*, *J. Mol. Biol.* **306**, 1099 (2001).
- [55] F. Fatehi and R. Twarock, *An interaction network approach predicts protein cage architectures in biotechnology*, *Proc. Natl. Acad. Sci. U.S.A.* **120**, e2303580120 (2023).
- [56] S. B. Rochal, O. V. Konevtsova, A. E. Myasnikova, and V. L. Lorman, *Hidden symmetry of small spherical viruses and organization principles in “anomalous” and double-shelled capsid nanoassemblies*, *Nanoscale* **8**, 16976 (2016).
- [57] G. Ueda *et al.*, *Tailored design of protein nanoparticle scaffolds for multivalent presentation of viral glycoprotein antigens*, *eLife* **9**, e57659 (2020).
- [58] C. Liang, K. Jiang, S. Tang, J. Wang, Y. Ma, W. Liu, and Y. Du, *Molecular-level insights into the nucleation mechanism of one-component soft matter icosahedral quasicrystal studied by phase-field crystal simulations*, *Cryst. Growth Des.* **22**, 2637 (2022).
- [59] W. Sheffler *et al.*, *Fast and versatile sequence-independent protein docking for nanomaterials design using RPxDock*, *PLoS Comput. Biol.* **19**, e1010680 (2023).
- [60] P. Plevka, K. Tars, and L. Liljas, *Crystal packing of a bacteriophage MS2 coat protein mutant corresponds to octahedral particles*, *Protein Sci.* **17**, 1731 (2009).
- [61] S. B. Rochal, O. V. Konevtsova, D. S. Roshal, A. Božič, I. Y. Golushko, and R. Podgornik, *Packing and trimer-to-dimer protein reconstruction in icosahedral viral shells with a single type of symmetrical structural unit*, *Nanoscale Adv.* **4**, 4677 (2022).
- [62] M. Martín-Bravo, J. M. Gomez Llorente, J. Hernández-Rojas, and D. J. Wales, *Minimal design principles for icosahedral virus capsids*, *ACS Nano* **15**, 14873 (2021).